THE ASTROPHYSICAL JOURNAL, 519:793–801, 1999 July 10

ALKALI ELEMENT CHEMISTRY IN COOL DWARF ATMOSPHERES

KATHARINA LODDERS
Planetary Chemistry Laboratory, Department of Earth and Planetary Sciences, Washington University, St. Louis, MO 63130-4899; lodders@levee.wustl.edu
Received 1998 May 28; accepted 1999 February 5

ABSTRACT

The equilibrium thermochemistry of the alkali elements in cool dwarf atmospheres is investigated as part of a comprehensive set of chemical equilibrium calculations. The abundances of all important gases and the condensation temperatures of all initial condensates for Li, Na, K, Rb, and Cs are calculated as a function of pressure and temperature. Also discussed is the chemistry of refractory elements such as Al, Ca, Cr, Fe, Mg, Si, Ti, and V. The calculation of the alkali element and refractory element chemistry can help to constrain pressure and temperature conditions in dwarf atmospheres. A relative temperature scale is developed and compared to recent observations of the alkali elements in late-type dwarfs and brown dwarfs, such as the DENIS objects and Gliese 229B. The calculations show (1) Atomic Li gas abundances are expected to be lower than the bulk Li abundance because LiOH gas (at high total pressure) or LiCl gas (at low total pressure) form in very cool objects. Observations of only monatomic Li are therefore not a good test for the substellar nature of very cool objects. (2) The observations of atomic Cs in Gliese 229B can be understood by considering the distribution of Cs between atomic Cs and CsCl gases. (3) Liquid condensates, which may form solutions with complex compositions, form at higher pressures, and need to be considered in further atmospheric structure and opacity modeling.

Subject headings: molecular processes — stars: abundances — stars: individual (Gliese 229B) — stars: low-mass, brown dwarfs

1. INTRODUCTION

In progressively cooler M dwarf atmospheres (>dM8), formation of elemental lines and molecular bands becomes increasingly more important. Of particular interest in cool dwarfs are TiO, VO, and the monatomic alkali elements, which can be used as temperature diagnostics. At temperatures reaching the very late dwarf to brown dwarf regime (>dM10), TiO and VO bands eventually disappear because Ti and V and other refractory elements such as Al, Ca, Cr, Fe, Mg, and Si are removed from the gas by condensates (e.g., Fegley & Lodders 1996; Tsuji et al. 1996b; Jones & Tsuji 1997). The less refractory alkali elements (Li, Na, K, Rb, Cs) then become prominent line producers and can serve as temperature diagnostics in cool dwarfs. As shown below, the alkali ions disappear with decreasing temperature and the neutral atoms become more abundant, with heavier alkalies showing this transition at the lowest temperatures.

Lithium is of particular interest because low-mass objects ($<0.065\ M_{\odot}$) are not expected to burn Li and high bulk abundances of Li can confirm the brown dwarf nature of a low-mass object (Rebolo, Martin, & Magazzu 1992). However, this Li test must be applied with caution because the abundance of Li (gas) can be reduced (below the bulk Li abundance of an object) by formation of other Li-bearing gases and/or formation of condensates. The applicability of the Li test is qualitatively addressed in the literature, but, so far, detailed thermochemical equilibrium calculations are available only for Jupiter (Fegley & Lodders 1994). Burrows & Sharp (1999) also addressed this issue, but in their calculations many refractory condensates continue to react with the gas to much lower temperatures (and hence higher altitudes) than predicted for condensate cloud formation in a Jovian planet atmosphere (cf. Lewis 1969, Barshay & Lewis 1978).

This paper describes thermochemical equilibrium calculations for Li, the other stable alkali elements (Na, K, Rb, Cs), and selected refractory elements that are important for interpreting spectra of low-mass dwarf stars and brown dwarfs. The computations lead to several important results, including a "phase diagram" showing where monatomic Li, different Li-bearing molecules, and Li-bearing condensates are the major reservoirs of lithium in brown dwarfs and cool stars. The calculations also provide a guide for interpreting observations of alkali elements in brown dwarfs and cool dwarf stars, in particular the observations of monatomic Cs in Gliese 229B, the coolest brown dwarf known. Preliminary results of this work were previously presented by Lodders (1998a, 1998b).

2. THERMOCHEMICAL EQUILIBRIUM CALCULATIONS

The calculations were performed using the CONDOR code described earlier (Fegley & Lodders 1994, 1996). The code contains ~2700 gaseous and solid compounds of all naturally occurring elements. Here a subset of the results for gas-phase and condensation chemistry of some major elements and the alkalies is reported. Computations were performed for a wide pressure-temperature (P-T) range for a solar composition gas and meteoritic abundances for Li, Be, and B (Lodders & Fegley 1998). The calculations simultaneously consider mass balance and chemical equilibrium. Some results of the calculations describing condensation of perovskite ($CaTiO_3$) Fe metal, and forsterite (Mg_2SiO_4), as well as the important CO-CH_4 and N_2-NH_3 boundaries relevant to brown dwarf atmospheres, were reported earlier (Fegley & Lodders 1996).

Mass balance requires refractory elements, which form condensates at high temperatures (i.e., deep in the brown dwarf atmosphere), to be absent from the gas at lower temperatures (e.g., see Barshay & Lewis 1978; Fegley & Lewis

1979; Fegley & Lodders 1994, 1996; Fegley & Prinn 1985a, 1985b, 1986; Lewis 1969). In other words, condensate cloud formation severely depletes the gas in refractory elements (e.g., Al, Ca, Ti, V, the lanthanides, Fe, Si, Mg) at higher altitudes where the temperatures are lower. Two independent sets of observations provide strong evidence for refractory element depletion via condensate formation deep in a planetary atmosphere.

First, the absence of SiH_4 and the presence of GeH_4 in the atmospheres of Jupiter and Saturn is due to depletion of refractory Si, but not of volatile Ge, by condensate formation deep in these atmospheres (Fegley & Lodders 1994). Silicon is much more abundant than Ge in a solar gas, and the atomic Si/Ge ratio is $10^6/120 \sim 8300$. However, SiH_4 is not observed on either Jupiter or Saturn, and the observational upper limits are $SiH_4/H_2 \sim 1 \times 10^{-9}$ by volume (ppbv). In contrast, GeH_4 is observed at $GeH_4/H_2 \sim 0.7$ ppbv on Jupiter and $GeH_4/H_2 \sim 0.4$ ppbv on Saturn (Lodders & Fegley 1998).

The second observation is the detection by the *Galileo* Probe Mass Spectrometer (GPMS) of H_2S at about 3 times the solar S/H ratio on Jupiter (Niemann et al. 1998). The calculations by Lewis (1969), Barshay & Lewis (1978), and Fegley & Lodders (1994), which consider depletion of Fe metal by condensate cloud formation deep in the atmospheres of Jupiter and Saturn, predict that H_2S will be present in the Jovian and Saturnian tropospheres below the NH_4SH cloud condensation level. The predictions of these calculations are in agreement with the GPMS observations of H_2S on Jupiter. Hydrogen sulfide has not yet been detected on Saturn, but the *CASSINI* spacecraft will probably be able to see below the NH_4SH clouds on Saturn and should detect H_2S in the Saturnian troposphere. However, calculations such as those by Burrows & Sharp (1999), which neglect refractory element depletion by condensate cloud formation, instead predict that H_2S would be totally absent from Jupiter's observable atmosphere because of formation of solid FeS (troilite) at 700 K. Condensation of FeS consumes all sulfur because the solar Fe/S ratio is about 2. The predicted formation of FeS and the consequent removal of H_2S is at odds with the GPMS observations. Thus, the absence of SiH_4 and the presence of GeH_4 on Jupiter and Saturn, and the GPMS observations of H_2S on Jupiter, support the condensation cloud modeling done here and by prior groups (Barshay & Lewis 1978; Fegley & Lewis 1979; Fegley & Lodders 1994, 1996; Fegley & Prinn 1985a, 1985b, 1986; Lewis 1969).

3. COMPUTATIONAL RESULTS

The results are presented in three figures to facilitate discussion. Figure 1 shows the effects of temperature on gas-phase chemistry at constant pressure. The less important gases of the alkali elements, Ca, Ti, V, Cr, and Fe, that appear in Figure 1 are omitted in subsequent figures for simplicity. Figure 2 shows the effects of temperature and pressure on the most abundant gases and on the condensates of all elements discussed here. Figure 3 addresses more details of Cs chemistry in Gliese 229B. Although the results are divided into three separate figures, all computations were complete thermochemical equilibrium calculations in which gases and condensates were considered.

3.1. *Effects of Temperature on Gas-Phase Chemistry*

Figure 1 shows the mole fractions of the most abundant gas-phase species of the alkali elements and of Ca, Ti, V, Cr, and Fe from 3300 to 1400 K at a total pressure of 1 bar (10^6 dyn cm^{-2}). This pressure falls within characteristic P ranges assumed for late dwarf and brown dwarf atmospheres (Marley et al., 1996; Tsuji, Ohnaka, & Aoki 1996a) and was chosen to illustrate trends. As a general rule, at constant temperature, higher pressures shift the gas-phase composition toward molecular species while lower pressures favor formation of monatomic and ionized species.

Lithium chemistry is shown in the top left of Figure 1. Monatomic Li is the major gas at high temperatures, and LiCl is the major Li-bearing gas below $\sim$1525 K. LiH and LiOH also increase in abundance with decreasing T, and at lower T than shown in Figure 1, LiOH becomes more abundant than LiCl from 1076 to 944 K. Lithium chemistry is discussed in more detail below.

The alkali elements Na and K are mainly present as neutral atoms over the temperature range shown in Figure 1. Hydrides, hydroxides, and chlorides become more abundant as temperature decreases but never become the most abundant gases at 1 bar total pressure. Although NaCl and KCl become increasingly important with decreasing T, their abundances never exceed the neutral Na or K abundance before Na_2S condensation (see Fig. 2).

Rubidium and cesium chemistry is illustrated at the top right in Figure 1. These elements have the lowest ionization potential of any naturally occurring element, and consequently Rb^+ and Cs^+ remain major gases down to temperatures where neutral Li, Na, and K are already the major gases for these alkalies. As T decreases, neutral Rb and Cs, and later, RbCl and CsCl, become the major gases, but RbH, CsH, RbOH, and CsOH are never very abundant at low T.

The gas chemistry of Ca, Ti, and V is shown at the lower left in Figure 1. The most abundant Ca gas prior to condensation is always atomic Ca, and Ca^+ does not become more abundant until higher T than shown. The next two most abundant gases, CaH and CaOH, are about 1.5–2 orders of magnitude less abundant than Ca gas. Above 2500 K, monatomic Ti and V are the dominant gases of these two elements. Their abundances drop with decreasing T as a result of increasing formation of TiO and VO, which eventually are removed by perovskite ($CaTiO_3$) condensation below 1957 K. Titanium is much less abundant than Ca, so perovskite condensation cannot remove all Ca from the gas. Other Ca-bearing condensates such as hibonite ($CaAl_{12}O_{19}$), grossite ($CaAl_2O_4$), or gehlenite ($Ca_2Al_2SiO_7$) condense within similar T ranges as perovskite or corundum (Al_2O_3), causing Ca removal from the gas. Vanadium is less refractory than Ti (Kornacki & Fegley 1986) and is removed from the gas by condensation into solid solution with perovskite at lower T.

The chemistry of Fe and Cr is shown at the bottom right in Figure 1. These elements are removed from the gas by metal condensation starting at 1840 K. Prior to condensation, monatomic Fe and Cr are the most abundant gases, followed respectively by FeH, FeS, and FeO and by CrO, CrS, and CrH. Note that the importance of the hydride and oxide for Fe and Cr are switched and that CrO (and CrS) are more abundant than CrH, while FeH is more abundant than FeO or FeS.

3.2. *Pressure Effects and Condensation Chemistry*

Figure 2 shows lines of equal abundances for the major

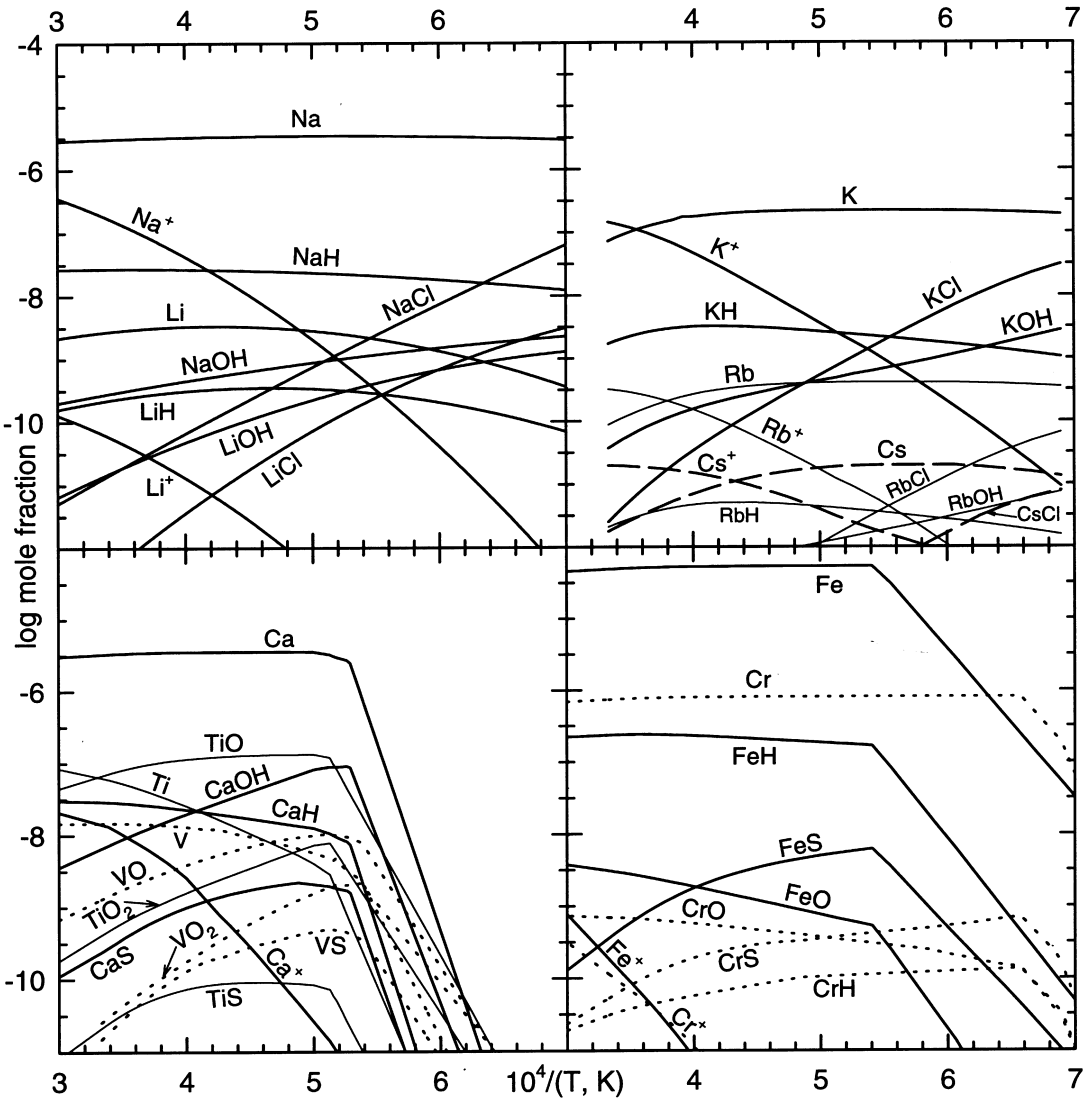

FIG. 1.—Abundances of major gases of the alkali elements, Ca, Ti, V, Fe, and Cr, as a function of temperature at 1 bar total pressure. Low temperatures favor formation of molecular species. The Ca, Ti, V, Fe, and Cr abundances decrease because these elements are removed from the gas by condensation.

gases of the alkalies, the CO/CH_4, and the N_2/NH_3 boundaries (*solid lines*) and condensation temperatures (*dashed lines*) as a function of total pressure and inverse temperature. The model atmospheres for an M dwarf ($T_{\rm eff}$ = 2200 K, dust-free; Tsuji et al. 1996a), Gliese 229B ($T_{\rm eff}$ = 960 K; Marley et al. 1996), and Jupiter are shown by dotted lines for reference. Jovian atmospheric chemistry is discussed by Fegley & Lodders (1994) and is slightly different from the chemistry of a solar composition gas because Jupiter is enriched in elements heavier than He relative to solar abundances.

Lithium chemistry is more sensitive to total pressure than the chemistry of the other alkali elements. The shaded regions in Figure 2 illustrate the fields where different Li-bearing gases are the most abundant Li species. (Note that Fig. 1 is a slice through Fig. 2 along the 1 bar isobar.) The dark gray region at the bottom of Figure 2 shows where monatomic Li is the dominant Li-bearing gas. The light gray regions show where LiCl is the dominant Li-bearing gas. The boundary between the dark gray and light gray region is the line where Li and LiCl have equal abundances. Likewise, the white region shows where LiOH is the dominant Li-bearing gas and the boundary between the dark gray and white region is the line where Li and LiOH have equal abundances. There is a triple point at 1641 K and 21.1 bar, where the Li, LiCl, and LiOH fields meet, and Li, LiCl, and LiOH each comprise one-third of the total Li abundance. The lightest gray region shows where LiF is the dominant Li-bearing gas. The white, light gray, and lightest gray regions meet near 918 K and 0.065 bar, where LiF, LiCl, and LiOH have equal abundances and each contains one-third of the total Li abundance. The LiF region is bounded on the top and bottom by the regions where LiCl is dominant.

Near the top of Figure 2 is another white region bounded by two dashed lines. These dashed lines are the condensation curves for solid Li_2S and solid LiF. The abundance of LiCl (the dominant Li-bearing gas at these pressures and temperatures) and the abundances of all Li-bearing gases are decreased by the condensation of these two solids.

Figure 2 shows that there is a relationship between Li chemistry and the $CO = CH_4$ boundary which lies close to the LiCl = LiOH boundary. LiOH is generally more important when CH_4 is more abundant than CO, and LiCl is

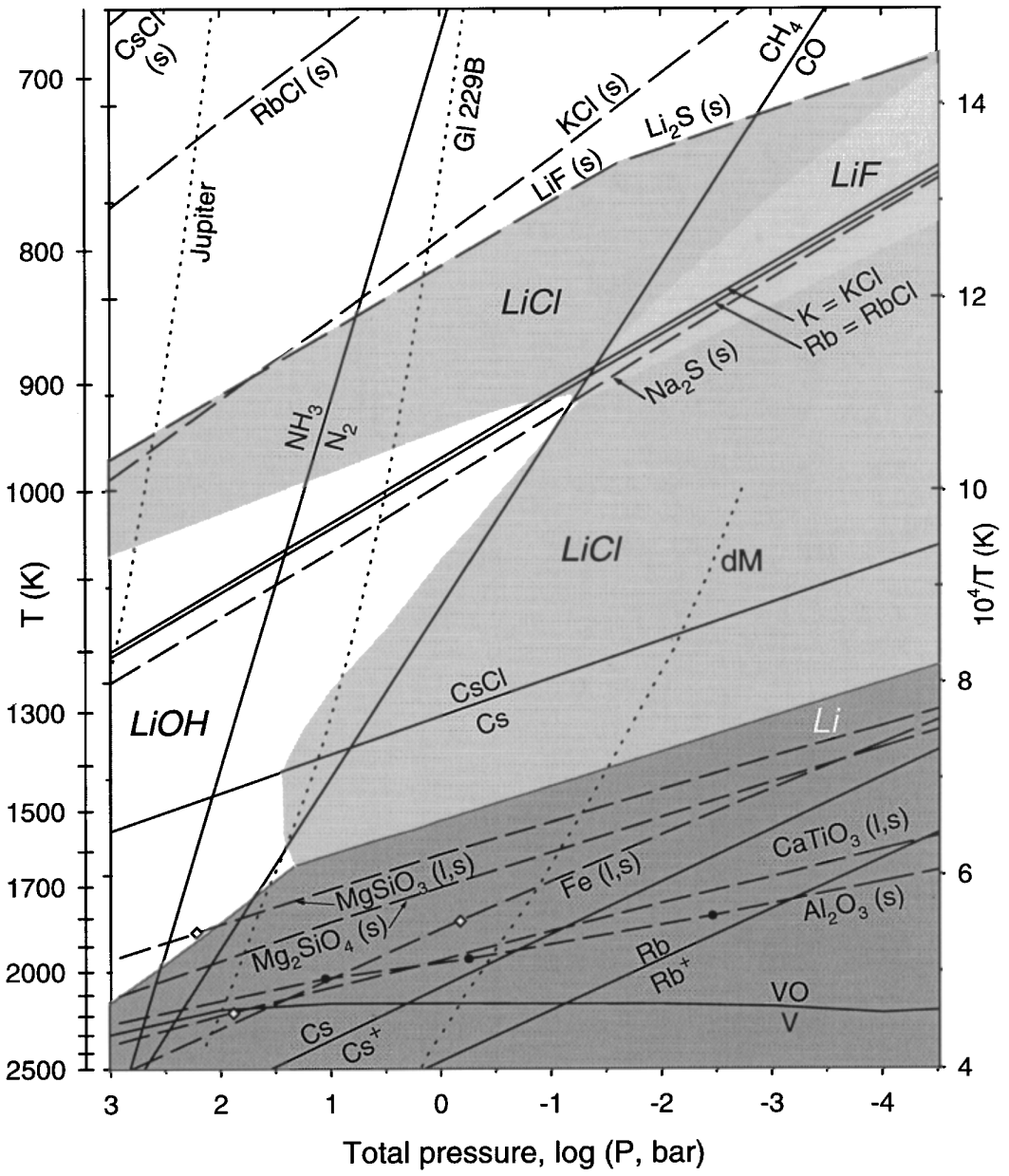

FIG. 2.—Temperature-pressure diagram showing lines where pairs of gaseous species have equal abundances (*solid lines*). For example, the line labeled CsCl = Cs shows where the CsCl and Cs mole fractions are equal; above the line, CsCl is more abundant than Cs. Also shown are the condensation temperatures of major element and alkali element condensates (*dashed lines*). The constituent condensate elements are removed from the gas above these lines. The corundum (Al_2O_3) condensation line shows which Al-bearing condensate forms as a function of total pressure. At low pressures, corundum forms. With increasing pressure, hibonite ($CaAl_{12}O_{19}$), Ca dialuminate ($CaAl_2O_4$), and gehlenite ($Ca_2Al_2SiO_7$) become the first Al-bearing condensates, and the transitions are indicated by the black dots on the corundum line. The white dots on the enstatite, perovskite, and forsterite condensation lines indicate melting points. The shaded areas indicate where Li, LiOH, LiCl, and LiF are the most abundant gases. The dotted lines are atmospheric *P-T* conditions in Jupiter, Gliese 229B (Marley et al. 1996), and an M dwarf ($T_{\rm eff}$ = 2200 K, dust-free; Tsuji et al. 1996a). See text for detailed explanation.

generally more important when CO is more abundant than methane. The reason for this is that more H_2O is available when CH_4 forms via $CO + 3H_2 = CH_4 + H_2O$, so that the reaction $LiCl + H_2O = LiOH + HCl$ also proceeds.

The condensation of Na_2S changes the Li gas chemistry, as well as that of Rb and K. Although monatomic Na is the most abundant Na-bearing gas, NaCl is the most abundant Cl-bearing gas at high temperatures before Na_2S condensation. At low T, after Na_2S condenses, the chlorine previously tied up in NaCl is released and KCl becomes the major Cl-bearing gas. Chlorine is about 1.4 times more abundant than K, and HCl is the second most abundant chlorine gas after KCl. Hydrogen chloride becomes the dominant Cl gas after KCl condenses. The increased availability of HCl after Na_2S condensation then allows conversion of LiOH (high P) or LiF (low P) to LiCl, which again becomes the major Li-bearing gas. Finally, LiCl is removed from the gas once solid LiF (high P) or Li_2S (low P) condenses at lower temperatures (Fig. 2 *top*, *white region*).

The chemistry of Na, K, Rb, and Cs is less complex than that of Li. Monatomic Na and K are more abundant than Na^+ and K^+ and are the major Na and K gases at the highest temperatures shown in Figure 2. Monatomic Na remains the dominant Na gas until Na_2S condensation. In

contrast, KCl becomes the dominant K-bearing gas at temperatures below the K = KCl line, and eventually solid KCl condensation occurs.

As mentioned earlier, Rb and Cs have the lowest ionization potentials of any naturally occurring element. The ions Rb^+ and Cs^+ are the dominant gases at the highest temperatures shown in Figure 2. The abundances of Rb^+ and Cs^+ decrease with decreasing temperature, and the abundances of Rb and Cs increase with increasing temperature until the lines labeled $Rb^+ = Rb$ and $Cs^+ = Cs$. Monatomic Rb and Cs are respectively more abundant below these two lines. Further decreases in temperature lead to decreases in the Rb and Cs abundances and to increases in the RbCl and CsCl abundances until the equimolar lines (Rb = RbCl and Cs = CsCl) are reached. Eventually gaseous RbCl and CsCl are depleted when solid RbCl and CsCl condense.

The Cs = CsCl transition occurs at higher temperatures before Na_2S condenses, as is the case for the Li = LiOH or Li = LiCl transitions. However, the Li = LiOH and Li = LiCl transitions are the first to occur with decreasing T. The Cs = CsCl transition occurs about 170–230 K lower (depending on total P) than the Li = LiCl transition.

The chemistry of some refractory elements is also shown in Figure 2. While the alkali-alkali chloride transitions are pressure dependent, the V-VO transition at relatively high temperatures ($\sim$2150 K) is essentially pressure independent, so the V/VO abundance ratio could serve as a good temperature indicator in M dwarfs. The more pressure-sensitive transition from Ti to TiO occurs at temperatures above 2500 K, so TiO is always the most abundant Ti-bearing gas for the conditions shown in Figure 2. The condensation temperatures of corundum, perovskite, Fe metal, forsterite, and enstatite ($MgSiO_3$) are also shown in Figure 2. The constituent elements are removed from the gas above these dotted lines. The corundum line is marked with black dots because, depending on total pressure, Al condenses into corundum or other Al-bearing phases. At pressures below 3.5×10^{-3} bar, corundum is the initial condensate. At higher pressures, corundum is replaced by other initial condensates: hibonite forms from 3.5×10^{-3} to 0.56 bar, grossite forms from 0.56 to 11.3 bar, and gehlenite is the initial condensate above 11.3 bar.

Here an important aspect of major element condensation needs to be mentioned. Models of dwarf atmospheres have become more sophisticated and include dust opacities (e.g., Tsuji et al. 1996a; Tsuji et al. 1996b). As shown in Figure 2, at higher pressures the condensation temperatures of several major element compounds are above their melting points. For example, Fe liquid forms at $T \geq 1809$ K, forsterite liquid at $T \geq 2163$ K, and enstatite liquid at $T \geq 1851$ K. The M dwarf model atmospheres by Tsuji et al. (1996a) consider solid dust formation but the derived P-T conditions fall into the stability fields of liquid condensates. The formation of solid dust particles or suspended liquid droplets (hazes or aerosols) can have different effects on atmospheric opacities and needs to be considered in atmospheric modeling. The liquid condensates may also dissolve other elements and have complex compositions.

4. A RELATIVE TEMPERATURE SCALE FOR M DWARFS AND BROWN DWARFS

The results in Figure 2 allow us to derive a relative temperature scale for M dwarfs and brown dwarfs based on the presence or absence of major element and alkali element gases in their atmospheres. These conclusions do not depend upon specific model atmospheres and can be used to constrain atmospheric models from observations of the different major element and alkali element gases in a given object.

We divide the relative temperature scale into five intervals by using the condensation temperature lines and lines of equal gas abundance in Figure 2. The highest temperature interval is bounded by the V = VO boundary. The next temperature interval is from the V = VO boundary to the perovskite condensation line. The next interval is from perovskite condensation to the Cs = CsCl boundary. This interval is subdivided by either the Li = LiCl or the Li = LiOH boundary. The next temperature interval is defined by the Cs = CsCl boundary and the Na_2S condensation line. The lowest temperature regime is below the Na_2S condensation line. Some examples of objects that fall into each temperature interval are given. The chemistry of Gliese 229B is discussed in a separate section.

4.1. *High Temperatures above the* V = VO *Boundary*

This interval is bounded by the V = VO line, which is at $\sim$2150 K over a wide range of pressures (see Fig. 2). The results in Figures 1 and 2 show that there are two important trends with increasing temperature in this interval. First, Ti and V become more abundant at the expense of TiO and VO. Second, Na^+, K^+, Rb^+, and Cs^+ become more abundant at the expense of the monatomic alkali gases.

These chemical trends are consistent for dwarfs earlier than $\sim$dM6.5, where molecular bands of TiO serve as classification criteria while dwarfs with increasingly stronger VO bands indicate spectral types later than dM6 (e.g., Kirkpatrick, Henry, & Liebert 1993; Leggett 1992). Figures 1 and 2 indicate that dwarfs with atomic Li, Na, K, and TiO (and to some extent VO) have atmospheric temperatures greater than 2150 K. The presence of atomic Rb and Cs then can provide constraints on the total pressure.

4.2. *Temperatures between the* V = VO *Boundary and the Perovskite Condensation Curve*

This interval is characterized by the condensation of refractory elements. The neutral atoms are the most abundant gases for all of the alkalies over this whole temperature range. Monatomic Ca, Fe, Cr, TiO, and VO are abundant.

Dwarfs with strong TiO and VO bands and lines of all neutral monatomic alkali elements are expected to have atmospheric temperatures between the V = VO boundary and the perovskite condensation curve. For these objects, the Li abundance derived from the Li I line is representative of the bulk Li abundance and can be used to decide an object's substellar nature. For example, the Pleiades brown dwarfs Teide 1 and Calar 3 have relatively strong TiO and VO bands, and their Li abundances are log $N(\mathrm{Li}) \geq 2.5$, clearly indicating their substellar nature, as concluded by Rebolo et al. (1996).

4.3. *Temperatures below Perovskite Condensation and above the* Cs = CsCl *Boundary*

This temperature interval is defined by the perovskite condensation curve and the Cs = CsCl boundary. Once perovskite condenses, TiO disappears from the gas and VO also disappears as vanadium condenses into perovskite. The removal of VO from the gas takes place at somewhat lower temperatures than TiO removal from the gas. Objects without any or with only weak TiO and VO bands and

displaying lines of all monatomic alkali elements have atmospheric temperatures cooler than the condensation temperature of perovskite, as expected from earlier thermochemical equilibrium calculations (e.g. Fegley & Lodders 1996; Jones & Tsuji 1997). The other refractory elements also condense into corundum and/or Ca, Al-bearing compounds, as well as forsterite, enstatite, and metal.

All alkali elements, except Li, are mainly present in their monatomic form. The Li = LiCl or Li = LiOH boundaries subdivide this interval, so that either Li (at the higher temperature end) or LiCl or LiOH (at the low-temperature end) are present together with neutral Na, K, Rb, and Cs.

The three field DENIS objects (DENIS-P J1228.2-1547, DENIS-P J1058.7-1548, and DENIS-P J0205.4-1159, hereafter respectively D12-1547, D10-1548, and D02-1159) investigated by Delfosse et al. (1997), Martin et al. (1997), and Tinney, Delfosse, & Forveille (1997) fall into the temperature ranges where perovskite condensation occurs. From D10-1548 to D12-1547 to D02-1159, TiO and VO bands get weaker with decreasing temperature, and these bands are essentially absent in D02-1159. The Cs line strength increases with decreasing temperature in all three objects and is strongest in D02-1159, consistent with the expectation that the neutral Cs abundance increases at the expense of ionic Cs. A similar situation occurs for Rb (Figs. 1 and 2). Lines of neutral Na and K seem to weaken systematically with decreasing temperatures (Tinney et al. 1997), plausibly because of the increasing formation of NaCl and KCl, although NaCl and KCl never become the major Na- and K-bearing gases before Na_2S condenses (Figs. 1 and 2). Unfortunately, molecular bands of the alkali chlorides are in the far-infrared, so that these potential temperature diagnostics are difficult to observe.

The presence of TiO, VO, and Cs for the hottest DENIS object D10-1548 suggest that atmospheric temperatures are in the range of 1900–2300 K (assuming total pressures of 0.1–100 bar; Fig. 2), so that this object actually falls into the temperature interval described in § 4.2 above. Atomic Li is expected in this temperature range because temperatures are higher than required for perovskite condensation (Fig. 2). The absence of atomic Li in D10-1548 implies that Li was destroyed by nuclear processing and, together with the weak Hα emission, suggests that D10-1548 is a very late M dwarf instead of a brown dwarf (Tinney et al. 1997).

Lithium is detected in D12-1547, and the presence of all neutral alkali elements suggests atmospheric temperatures between about 1450 and 1850 K (for $P = 0.1$ bar) or between 1820 and 2200 K (for $P = 100$ bar), as indicated from the perovskite condensation temperature curve and the Li = LiOH or Li = LiCl boundaries in Figure 2. The presence of Li in the spectrum of D12-1547 makes it a bona fide brown dwarf and also constrains its atmospheric temperature regime. Another object, GD 165B, seems to fall in between D12-1547 (brown dwarf) and D10-1548 (very late dM), but unfortunately the Li I line sits in a spectral region that is contaminated by light from the white dwarf companion GD 165A, so that the Li test cannot be applied to GD 165B (see e.g., Martin et al. 1997; Tinney et al. 1997). However, weak or absent VO and TiO bands combined with strong Rb and Cs lines should be useful to at least constrain whether or not atmospheric temperatures are below the perovskite condensation temperature.

In the coolest DENIS object, D02-1157, TiO and VO are essentially absent, and monatomic Na, K, Rb, and Cs are present. Unfortunately, the presence or absence of Li is currently not known for D02-1159 (Tinney et al. 1997). If temperatures in D02-1157 are above the Li = LiCl or Li = LiOH boundary, monatomic Li is expected. The absence of neutral Li in this case would indicate Li-burning, so that D02-1157 is a very cool stellar object. On the other hand, at lower temperatures, most of the Li is present as LiOH or LiCl and the bulk Li abundance derived from the Li I line must be too low. In low-temperature objects the absence or presence of LiOH or LiCl is a better indicator for the bulk Li abundance and for constraining an object's stellar or substellar nature. The presence of neutral Cs is no guarantee that the neutral Li can serve as a proxy for the bulk Li abundance because neutral Cs is still the most abundant Cs-bearing gas at temperatures where LiCl (or LiOH) has replaced Li as the most abundant Li-bearing gas.

4.4. *Temperatures below the* Cs = CsCl *Boundary and above* Na_2S *Condensation*

This range spans temperatures from ~1250 to ~930 K (0.1 bar) or from ~1450 to ~1150 K (100 bar). In this interval, TiO, VO, and refractory major elements are absent. Monatomic Na and K dominate, although their chlorides become increasingly abundant with decreasing temperature. Monatomic Rb is the most abundant Rb gas. LiOH or LiCl are more abundant than Li, and the abundance of atomic Li cannot be used as a proxy of the total Li abundance for the Li test. CsCl is the most abundant Cs-bearing gas. Objects characteristic for this temperature interval are expected to show monatomic Na, K, and Rb but no Li, Cs, VO and TiO. Currently, no objects with these characteristics are reported. However, the brown dwarf Gliese 229B may fall into this or the next lower temperature interval, as discussed in § 5.

4.5. *Temperatures below* Na_2S *Condensation*

The lowest temperature interval is characterized by the absence of monatomic Na because temperatures are below the condensation temperature of Na_2S (*solid*). Below this temperature, KCl, RbCl, CsCl, and LiOH, LiF, or LiCl are the most abundant alkali gases, and abundances of monatomic K and Rb drop with decreasing temperature. LiCl is removed from the gas when LiF or Li_2S condenses (at lower T than Na_2S condensation); and, similarly, KCl gas disappears because of KCl (*solid*) condensation at even lower T. In the latter case, only RbCl and CsCl remain in the gas, and their presence or absence indicates temperatures above or below the condensation temperatures of RbCl (*solid*) and CsCl (*solid*), respectively. Objects falling into this temperature range are the gas giant planets such as Jupiter.

5. ALKALI CHEMISTRY IN GLIESE 229B

The thermochemical equilibrium calculations are now used to discuss the alkali element chemistry of Gliese 229B, the coolest brown dwarf known to date. Monatomic Cs is the only alkali element detected in the atmosphere of Gliese 229B (Oppenheimer et al. 1998; Schultz et al. 1998). Calculations in Figures 1 and 2 show that monatomic Cs should be accompanied at least by monatomic Na, K, and Rb, because the Cs = CsCl transition occurs at a higher temperature than the Rb = RbCl, or K = KCl transition (Fig. 2). However, only one Cs line (0.8944 μm) was detected in the

optical spectrum taken by Schultz et al. (1998), although the strongest Li, Na, K, and Rb lines are also expected in the spectral range observed. The high-resolution spectrum by Oppenheimer et al. (1998) shows two Cs lines (0.8521 and 0.8944 μm), but their spectrum does not extend to lower wavelengths, where Na, K, Rb, and Li are located. Some weaker lines of Na, K, and Rb are located in the spectral range covered by the high-resolution near-infrared spectrum taken by Geballe et al. (1996), but the strong water and methane bands in this spectral range complicate detection of any Na, K, or Rb lines.

The detection of Cs in the cool atmosphere of Gliese 229B with an effective temperature of about 950 K is unusual because at these temperatures Cs is mainly present as CsCl (Fig. 2). At these temperatures, all other monatomic alkalies are also expected to be absent from the atmosphere of Gliese 229B. Using the Gliese 229B *P-T* profile in Figure 2, we find that sodium sulfide condenses at 1033 K and that KCl (gas) and RbCl (gas) then become the most abundant K- and Rb-bearing gases. The major Li-bearing gas is either LiOH or LiCl. Taking the *P-T* profile for Gliese 229B at face value, the abundant Li-bearing gases with decreasing temperature are Li, LiOH, LiCl, LiOH, LiCl, until removal by LiF solid condensation.

The detection of Cs lines does not necessarily mean that most Cs is present as monatomic Cs gas. Without a measurement of the monatomic Cs abundance, we do not know whether Cs gas or CsCl gas is the dominant Cs reservoir. The determination of the atomic Cs abundance and the question of what are the detection limits for atomic Cs and the other monatomic alkalies in brown dwarf atmospheres are important issues that need to be addressed by spectroscopists.

There are three possible explanations for the observation of monatomic Cs in Gliese 229B. (*a*) Some Cs is still present in the atmosphere of Gliese 229B, although CsCl is the major Cs-bearing gas at the low effective temperatures of 950–1000 K. Thus, we need to investigate the distribution of Cs between Cs gas and CsCl gas as a function of temperature and pressure. (*b*) The observations probe deeper levels of the atmosphere of Gliese 229B. (*c*) Monatomic Cs is mixed from the lower to the upper atmosphere. As discussed below, the last possibility is unlikely. The first explanation is given preference here, but until more information about the presence or absence of the other monatomic alkali elements and the alkali chlorides is available, the second possibility cannot be ruled out.

5.1. *Observation of Atomic* Cs *Probes Regions Where* CsCl *Is the Dominant Gas*

Figure 3 shows the calculated distribution of Cs between atomic Cs and CsCl as a function of P and T. The partial pressure (p_i) of Cs and CsCl are plotted as a function of temperature for different total pressures ($p_i = X_i P_{\rm tot}$, where X_i is the mole fraction). Figure 3 shows that the Cs = CsCl transition temperature (i.e., the intersection of the solid and dotted lines) increases with increasing pressure. This is also shown in Figure 2. The transition of Cs to CsCl occurs at $\sim$950 K at 10^{-7} bar, increasing to $\sim$1550 K at 10^{3} bar. At a given pressure, the Cs (gas) abundance does not drop rapidly with decreasing temperature, and some Cs (gas) is still present at low T, where CsCl is the dominant Cs-bearing gas. The Cs (gas) abundance decreases less steeply at lower pressures than at higher pressures. The steep drops

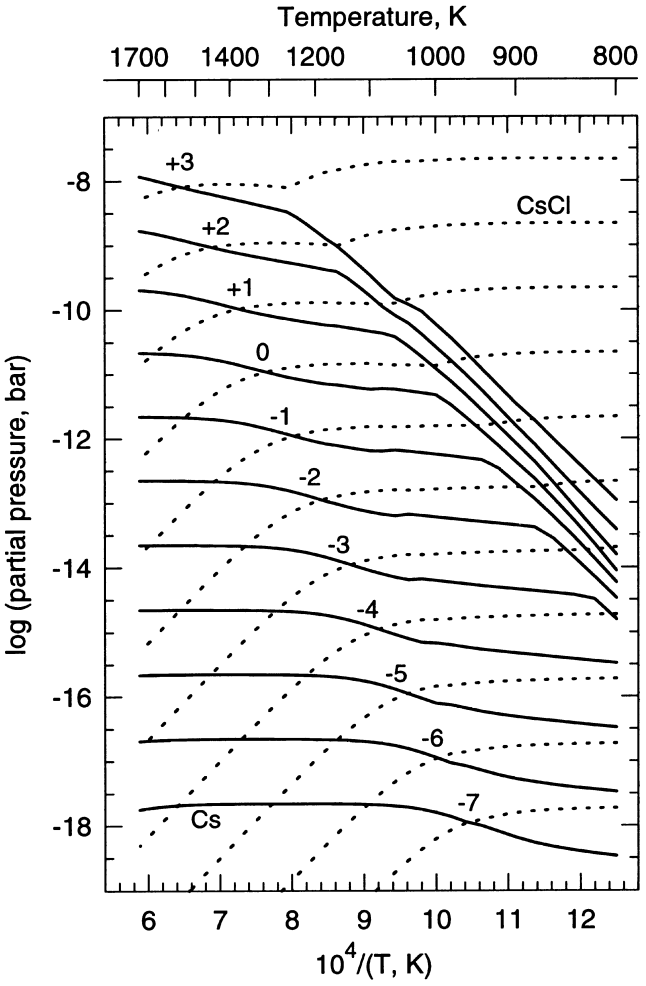

FIG. 3.—Distribution of Cs between Cs gas and CsCl gas as a function of temperature and total pressure. The abundances of Cs and CsCl are plotted as solid and dotted lines, respectively. The total pressure, in log [P (bar)], is indicated for each Cs and CsCl pair. Formation of CsCl occurs at the expense of monatomic Cs. The intersections of the solid and dotted lines show the Cs = CsCl boundary. The Cs–CsCl transition temperatures increase with increasing pressure. At low temperatures CsCl gas is the more abundant Cs-bearing gas, but a significant drop in the Cs gas abundance does not occur until temperatures are much lower than that of the Cs = CsCl boundary. This behavior is pronounced at low pressures. Partial pressures p_i equal X_i P, where X_i is the mole fraction and P is the total pressure.

in the Cs abundance are caused by condensation of Na_2S and by the subsequent increase of Cl in the gas, which increases the CsCl partial pressure. Atomic Cs, although not the major Cs-bearing gas, is still abundant in the temperature interval between the Cs = CsCl boundary and the Na_2S condensation curve in Figure 2.

To apply the calculations from Figure 3 to Gliese 229B, we can look at total pressures where the Cs abundance does not drop rapidly below the Cs = CsCl boundary down to temperatures of 950 K. For example, at total pressures smaller than 0.1 bar, the Cs abundances are always within a factor of 2 of the CsCl abundance. However, these low pressures are apparently not applicable to the *P-T* profile of Gliese 229B. At higher total pressures, the Cs abundances drop steeply when sodium sulfide condenses, so that the amount of atomic Cs decreases more rapidly in the 950–1000 K range.

According to the *P-T* profile of Gliese 229B shown in Figure 2, the total pressure in the 950–1000 K range is about 3 bar, where 10% or less of all Cs is present as atomic Cs. In principle, the Cs abundance and the Cs/CsCl abundance ratio can serve as temperature and pressure indicators provided that Cs abundances can be determined and that CsCl can be detected in the far-infrared and a CsCl abundance can be derived.

The condensation temperature of Na_2S at 1033 K (about 3.5 bar) is also very close to this temperature range, so that atomic Na, as well as atomic K and Rb, are depleted in the 950–1000 K range (Fig. 2), which can complicate their spectroscopic detection. However, the Na, K, and Rb abundances do not drop immediately to very low values. For example, Rb (gas) should be present in the temperature range where atomic Cs is still $\geq$ 1% of total Cs. As seen from Figure 2, the Rb = RbCl boundary is located at much lower T than the Cs = CsCl boundary. As a rule, the Rb/RbCl ratio at a given temperature and pressure is always larger than the Cs/CsCl ratio. Rubidium may be detectable in Gliese 229B in high-resolution spectra covering the range where the Rb 0.7800 and 0.7948 μm absorption lines are located, and weaker lines of atomic Na and K may also be visible in high-resolution spectra. Only monatomic Li is already very depleted because LiOH and/or LiCl comprise more than 99% of all Li at 950–1000 K, whereas the other alkalies still have at least a few percent in their monatomic form.

5.2. *Observations of Atomic* Cs *Probe a Deeper Atmosphere Level in Gliese 229B*

An alternative explanation of the observation of atomic Cs is that the observations probe to deeper levels of the atmosphere. Oppenheimer et al. (1998) estimate a brightness temperature of about 1300 K for the spectral region where the Cs lines are located. This temperature is not too far from the Cs = CsCl boundary for the *P-T* profile of Gliese 229B (1390 K and 13.1 bar) in Figure 2. As discussed above, atomic Cs is still present after CsCl becomes the major Cs-bearing gas, and if it is possible to determine the abundances of Cs and CsCl, we would have the possibility of refining determinations of the temperature. This case also implies that atomic lines of the other alkali elements falling into this spectral range should also be present.

5.3. *Mixing of* Cs *to the Upper Atmosphere in Gliese 229B*

The third alternative to explain the atomic Cs is to invoke convective mixing from the deep atmosphere to higher (visible) parts of the atmosphere. Such mixing is known on Jupiter for species such as Co, PH_3, AsH_3, or GeH_4 and is possible because the chemical reactions destroying these species are quenched deeper in the atmosphere. Thus, these compounds are mixed upward and are present in higher abundance than expected from thermochemical equilibrium (see Fegley & Lodders 1994 for details). Burrows & Sharp (1999) discuss the possibility that the presence of Cs in Gliese 229B is due to convection. However, preliminary calculations show that the timescales for reactions of alkali atoms to alkali chlorides are much faster than plausible mixing timescales (assuming similar mixing timescales on Gliese 229B to those on Jupiter), so that atomic Cs (and other atomic alkalies) cannot be quenched and Cs instead reacts to form CsCl.

6. SUMMARY

Detailed thermochemical equilibrium gas-phase and condensation calculations over a wide *P-T* range are presented. A relative temperature scale is developed based on the presence or absence of abundant gases of major and alkali elements. This temperature scale is compared with observations of alkali elements in M dwarf and brown dwarf atmospheres. The results show that the Li abundance obtained from Li I lines is only representative of the bulk Li abundance at pressures and temperatures where monatomic Li is more abundant than LiOH or LiCl gas. The presence of TiO and VO or of all monatomic alkali elements in an object indicates that temperatures are high enough to use the Li I lines as a proxy of the Li abundance to test the substellar nature of low-mass objects.

Lithium is the first alkali element converting from atomic to molecular species at high temperatures. A small temperature interval exists where Na, K, Rb, and Cs are in their monatomic form and LiOH (at high total P, when CH_4 is abundant) or LiCl (at low total P, when CO is abundant) is more abundant than Li gas. In this case the bulk Li abundance derived from atomic Li is too low and could cause a mis-classification of a brown dwarf as a low-mass star. The abundances of LiOH, LiCl, or LiF are better suited for Li abundance determinations and help to constrain atmospheric pressure and temperature.

The chemistry of Gliese 229B is discussed in more detail, and the need for observations of all alkali elements in its atmosphere is indicated. The calculations show that the presence and abundances of alkali element species place constraints on the temperature and pressure regime in atmospheres of cool low-mass objects. Ideally, searches and abundance determinations for monatomic and chloride species of all alkali elements are desirable because their abundance ratios can serve as temperature diagnostics in brown dwarf atmospheres.

The equilibrium calculations show that condensates of major elements at high pressures are liquids (e.g., Fe metal, forsterite, enstatite), which may form solutions with complex compositions. Such liquid condensates need to be considered in atmospheric modeling.

Work supported by NAG5-6366 from the NASA Planetary Atmospheres Program. I thank B. Fegley for helpful discussions and M. Marley for useful comments.

REFERENCES

Barshay, S. S., & Lewis, J. S. 1978, Icarus, 33, 593
Burrows, A., & Sharp, C. M. 1999, ApJ, 512, 843
Delfosse, X., et al. 1997, A&A, 327, L25
Fegley, B., Jr., & Lewis, J. S. 1979, Icarus, 38, 166
Fegley, B., & Lodders, K. 1994, Icarus, 110, 117
———. 1996, ApJ, 472, L37
Fegley, B., Jr., & Prinn, R. G. 1985a, Nature, 318, 48
———. 1985b, ApJ, 299, 1067
———. 1986, ApJ, 307, 852
Geballe, T. R., Kulkarni, S. R., Woodward, C. E., & Sloan, G. C. 1996, ApJ, 467, L101
Jones, H. R. A., & Tsuji, T. 1997, ApJ, 480, L39
Kirkpatrick, J. D., Henry, T. J., & Liebert, J. 1993, ApJ, 406, 701
Kornacki, A. S., & Fegley, B., Jr. 1986, Earth Planet. Sci. Lett., 79, 217
Leggett, S. K. 1992, ApJS, 82, 351
Lewis, J. S. 1969, Icarus, 10, 393
Lodders, K. 1998a, EOS Trans. AGU, 79, W56
———. 1998b, BAAS, 30, 1057

Lodders, K., & Fegley, B. 1998, The Planetary Scientist's Companion (New York: Oxford Univ. Press)
Marley, M. S., Saumon, D., Guillot, T., Freedman, R. S., Hubbard, W. B., Burrows, A., & Lunine, J. I. 1996, Science, 272, 1919
Martin, E. L., Basri, G., Delfosse, X., & Forveille, T. 1997, A&A, 327, L29
Niemann, H. B., et al. 1998, J. Geophys. Res. 103, E22831
Oppenheimer, B. R., Kulkarni, S. R., Matthews, K., & van Kerwijk, M. H. 1998, ApJ, 502, 932
Rebolo, R., Martin, E. L., Basri, G., Marcy, G. W., & Zapatero-Osorio, M. R. 1996, ApJ, 469, L53
Rebolo, R., Martin, E. L., & Magazzu, A. 1992, ApJ, 289, L83
Schultz, A. B., et al., 1998, ApJ, 492, L181
Tinney, C. G., Delfosse, X., & Forveille, T. 1997, ApJ, 490, L95
Tsuji, T., Ohnaka, K., & Aoki, W. 1996a, A&A, 305, L1
Tsuji, T., Ohnaka, K., Aoki, W., & Nakajima, T. 1996b, A&A, 308, L29